

Interaction between Fast and Ultra-slow Inactivation in the Voltage-gated Sodium Channel

DOES THE INACTIVATION GATE STABILIZE THE CHANNEL STRUCTURE?*

Received for publication, June 7, 2002, and in revised form, July 10, 2002
Published, JBC Papers in Press, July 23, 2002, DOI 10.1074/jbc.M205661200

Karlheinz Hilber^{‡§}, Walter Sandtner^{‡§}, Oliver Kudlacek[‡], Blanca Schreiner[‡], Ian Glaaser[¶],
Wolfgang Schütz[‡], Harry A. Fozzard[¶], Samuel C. Dudley[¶], and Hannes Todt^{‡**}

From the [‡]Institute of Pharmacology, University of Vienna, A-1090 Vienna, Austria, the [¶]Cardiac Electrophysiology Laboratories, The University of Chicago, Chicago, Illinois 60637, and the [¶]Division of Cardiology, Emory University, Atlanta, Georgia 30033 and the Atlanta Veterans Affairs Hospital, Decatur, Georgia 30033

Recently, we reported that mutation A1529D in the domain (D) IV P-loop of the rat skeletal muscle Na⁺ channel μ_1 (DIV-A1529D) enhanced entry to an inactivated state from which the channels recovered with an abnormally slow time constant on the order of ~100 s. Transition to this “ultra-slow” inactivated state (USI) was substantially reduced by binding to the outer pore of a mutant μ -conotoxin GIIIA. This indicated that USI reflected a structural rearrangement of the outer channel vestibule and that binding to the pore of a peptide could stabilize the pore structure (Hilber, K., Sandtner, W., Kudlacek, O., Glaaser, I. W., Weisz, E., Kyle, J. W., French, R. J., Fozzard, H. A., Dudley, S. C., and Todt, H. (2001) *J. Biol. Chem.* 276, 27831–27839). Here, we tested the hypothesis that occlusion of the inner vestibule of the Na⁺ channel by the fast inactivation gate inhibits ultra-slow inactivation. Stabilization of the fast inactivated state (FI) by coexpression of the rat brain β_1 subunit in *Xenopus* oocytes significantly prolonged the time course of entry to the USI. A reduction in USI was also observed when the FI was stabilized in the absence of the β_1 subunit, suggesting a causal relation between the occurrence of the FI and inhibition of USI. This finding was further confirmed in experiments where the FI was destabilized by introducing the mutations I1303Q/F1304Q/M1305Q. In DIV-A1529D + I1303Q/F1304Q/M1305Q channels, occurrence of USI was enhanced at strongly depolarized potentials and could not be prevented by coexpression of the β_1 subunit. These results strongly suggest that FI inhibits USI in DIV-A1529D channels. Binding to the inner pore of the fast inactivation gate may stabilize the channel structure and thereby prevent USI. Some of the data have been published previously in abstract form (Hilber, K., Sandtner, W., Kudlacek, O., Singer, E., and Todt, H. (2002) *Soc. Neurosci. Abstr.* 27, program number 46.12).

Voltage-gated Na⁺ channels mediate the Na⁺ conductance responsible for the rapidly rising phase of the action potential in nerve and muscle cells. Upon repolarization from brief depolarizations (<50 ms), Na⁺ channels recover from inactivation with a single kinetic phase whose time constant is on the order of a few milliseconds. After long depolarizations (seconds to minutes), recovery from inactivation proceeds through multiple kinetic phases whose time constants range over several orders of magnitude up to tens of seconds (1, 2). The most rapid phase of recovery is thought to correspond to the process of exit from the fast inactivated state, which occurs via intracellular occlusion of the ion-conducting pore by a cluster of hydrophobic amino acids in the loop that links DIII and DIV, the so-called “fast inactivation gate” of the Na⁺ channel (3, 4). All other kinetic phases of recovery have been associated with a relatively poorly understood process called “slow inactivation.” The physiological importance of slow inactivation was established when defects in slow inactivation were found to underlie the pathophysiology of a number of heritable diseases of skeletal muscle (5–10), heart (11–13), and brain (14).

We recently demonstrated that replacement of alanine 1529 by aspartic acid in the DIV P-loop of the rat skeletal muscle Na⁺ channel μ_1 (DIV-A1529D) enhanced entry to an ultra-slow inactivated state, which is characterized by time constants of entry to and recovery from inactivation of ~100 s (1). A similar type of recovery from inactivation in μ_1 channels with slow time constants on the order of several tens of seconds was reported recently by other authors (*e.g.* Refs. 9 and 15). In DIV-A1529D channels, transition to this ultra-slow inactivated state was substantially reduced by binding to the outer pore of a mutant μ -CTX.¹ This suggested that ultra-slow inactivation may reflect a structural rearrangement of the outer channel vestibule and that binding to the pore of a peptide can stabilize the pore structure (1, 16).

Although the structural determinants of fast inactivation are distinct from those of slow inactivation (*e.g.* Refs. 17 and 18), the various inactivation processes seem to be coupled. Fast inactivation inhibits the probability of slow inactivation (7, 17, 19, 20), probably via gating charge immobilization (21). Similarly, ultra-slow inactivation may as well be modulated by other types of inactivation. However, the effects of faster types of inactivation on ultra-slow inactivation have not yet been investigated.

μ_1 Na⁺ channels consist of a pore-forming α subunit and an auxiliary β_1 subunit. Coexpression of β_1 subunits with μ_1 α subunits in *Xenopus* oocytes modulates the gating properties of the channels (22, 23). The most dramatic β_1 effect is an in-

* This work was supported by Fonds zur Förderung der Wissenschaftlichen Forschung Grant P13961-MED (to H. T.), by National Institutes of Health Grant HL-P01–20592 (to H. A. F.), by an American Heart Association Southeast Affiliate Beginning grant-in-aid (to S. C. D.), by a Scientist Development Award from the American Heart Association, by a Procter and Gamble University Research Exploratory Award, and by National Institutes of Health Grant HL64828. The costs of publication of this article were defrayed in part by the payment of page charges. This article must therefore be hereby marked “advertisement” in accordance with 18 U.S.C. Section 1734 solely to indicate this fact.

§ These authors contributed equally to this work.

** To whom correspondence should be addressed: Institute of Pharmacology, University of Vienna, Währingerstrasse 13A, A-1090 Vienna, Austria. Tel.: 43-1-4277-64120; E-mail: hannes.todt@univie.ac.at.

¹ The abbreviations used are: μ -CTX, μ -conotoxin GIIIA; D, domain.

crease in the rate of inactivation, which is reflected by an acceleration of the current decay after channel activation. β_1 exerts its effects by stabilization of the fast inactivated state (e.g. Refs. 24 and 25). In the presence of β_1 , the channels favor a "fast-gating mode" in which they open only once or twice per depolarizing prepulse. In the absence of β_1 , the fast inactivated state is destabilized, and a "slow-gating mode" predominates that is reflected by bursts of channel openings (23, 26, 27).

In a previous study (1), we found that coexpression of the rat brain β_1 subunit slowed entry of DIV-A1529D channels to the ultra-slow inactivated state during long-lasting depolarizations. This result and the fact that the β_1 subunit stabilizes the fast inactivated state suggested that fast inactivation could inhibit ultra-slow inactivation. This hypothesis was investigated in the present study. Therefore, we explored the effects of stabilization and destabilization of the fast inactivated state on ultra-slow inactivation. We found strong evidence that fast inactivation inhibits entry to the ultra-slow inactivated state, possibly because binding to the inner pore of the fast inactivation gate stabilizes the channel structure.

EXPERIMENTAL PROCEDURES

A detailed description of the experimental procedures is given in our previous work (1).

Mutagenesis of the μ_1 —The oligonucleotide-directed point mutation DIV-A1529D was introduced using four-primer PCR. An oligonucleotide containing the mutation was designed with a change in a silent restriction site to allow rapid identification of the mutant. A vector consisting of the μ_1 -coding sequence flanked by *Xenopus* globin 5'- and 3'-untranslated regions was provided as a gift by R. Moorman. This was used as the template for mutagenesis, and PCR fragments were isolated and subcloned to this template using directional ligations. Incorporation of the mutation was confirmed by DNA sequencing of the entire polymerized regions. The vector was linearized by *SalI* digestion and transcribed with SP6 DNA-dependent RNA polymerase using reagents from the mCAP RNA capping kit (Stratagene, La Jolla, CA). The rat brain β_1 subunit of the Na⁺ channel was also subcloned into pAlterXG, and transcription was prepared from *Bam*H1-linearized template using SP6 RNA polymerase.

Mutagenesis of DIV-A1529D + I1303Q/F1304Q/M1305Q—I1303Q/F1304Q/M1305Q was made by oligonucleotide-directed mutagenesis and confirmed by sequencing the polymerized region. DIV-A1529D was introduced in this construct by cloning the *Sac*II-*Kpn*I fragment into the I1303Q/F1304Q/M1305Q construct. The presence of both mutations in the final plasmid was confirmed by restriction digests analyzing silent mutations introduced at the time of mutagenesis.

Stage V and VI *Xenopus* oocytes were isolated from female frogs (NASCO, Ft. Atkinson, WI), washed with Ca²⁺-free solution (90 mM NaCl, 2.5 mM KCl, 1 mM MgCl₂, 1 mM NaHPO₄, and 5 mM HEPES titrated to pH 7.6 with 1 N NaOH), and treated with 2 mg/ml collagenase (Sigma) for 1.5 h; follicular cell layers were manually removed. As judged from photometric measurements, ~50–100 ng of cRNA was injected into each oocyte with a Drummond micro-injector (Broomall, PA). Either native or mutant α subunit cRNA alone or mixed with various concentrations of rat brain β_1 subunit were injected. In the case of DIV-A1529D channels, the injected molar cRNA α/β_1 ratio ranged from 100 to 0.07. Oocytes were incubated at 17 °C for 12 h to 3 days before examination.

Recordings were made in the two-electrode voltage clamp configuration using a TEC 10CD clamp (npi electronic, Tamm, Germany). The clamp amplifier had a series compensation circuit. For accurate adjustment of the experimental temperature (20 ± 0.5 °C) an oocyte bath cooling system (HE 204, Dagan, Minneapolis, MN) was used. Oocytes were placed in recording chambers in which the bath flow rate was about 100 ml/h, and the bath level was adjusted so that the total bath volume was less than 500 μ l. Electrodes were filled with 3 M KCl and had resistances of less than 1 megaohm. Using pCLAMP6 (Axon Instruments, Foster City, CA) software, data were acquired at 71.4 kHz after low-pass filtration at 2 kHz (–3 decibel). Curve fitting was performed using ORIGIN 5.0 (MicroCal Software, Inc., Northampton, MA). Recordings were made in a bathing solution that consisted of 90 mM NaCl, 2.5 mM KCl, 1 mM BaCl₂, 1 mM MgCl₂, and 5 mM HEPES titrated to pH 7.2 with 1 N NaOH. BaCl₂ was used as a replacement for CaCl₂ to minimize Ca²⁺-activated Cl[–] currents.

Data Evaluation—If not otherwise specified, recovery from ultra-slow inactivation was tested with the following experimental protocol. From a holding potential of –120 mV, the channels were inactivated by a 300-s depolarizing voltage step. Thereafter, the potential was returned to –120 mV, and recovery from inactivation was monitored by repetitive 25-ms test pulses to –20 mV at 20-s intervals. The first test pulse was applied 3–10 ms after the prepulse to allow for settlement of the capacitive current transients. The time courses of recovery from ultra-slow inactivation of normalized peak inward currents were fit with the double exponential function,

$$I_2/I_1 = -A_1 \exp(-t/\tau_1) - A_2 \exp(-t/\tau_2) + C \quad (\text{Eq. 1})$$

where I_2 is the peak inward Na⁺ current of the test pulse during recovery, I_1 is the peak inward Na⁺ current of a test pulse under fully available conditions, τ_1 (always constrained to 10–12 s) and τ_2 (always constrained to 100–150 s) are the time constants of distinct components of recovery, A_1 and A_2 are the respective amplitudes of these time constants, and C is the final level of recovery. A_2 was taken as a measure of the fraction of channels that recovered from ultra-slow inactivation (see Ref. 1) and will subsequently be referred to as "ultra-slow fraction." In the case of the mutant μ_1 -I1303Q/F1304Q/M1305Q, which did not exhibit ultra-slow inactivation, recovery from slow inactivation was fit with the monoexponential function.

$$I_2/I_1 = -A \exp(-t/\tau) + C \quad (\text{Eq. 2})$$

The kinetics of the current decay after activation by a step depolarization was taken as a measure of the fraction of DIV-A1529D channels, which inactivated fast (time constants about 1 ms ("fast-gating channels") or slow (time constants >10 ms ("slow-gating channels")). We consider a large fraction of fast-gating channels to reflect a high degree of stabilization of the fast inactivated state (24, 25). The current decay was analyzed using two different methods.

First, the current decay after channel activation was fit by a bi-exponential function (Equation 1). The two different amplitudes (A_1 and A_2) were taken as a measure of the fraction of channels that gated either fast (A_1) or slow (A_2), respectively. If not otherwise specified, the channels were activated with the voltage step that elicited maximum current. For accurate comparison of the time constants of current decay in DIV-A1529D α -only and DIV-A1529D $\alpha + \beta_1$ channels, it was essential to precisely adjust the bath temperature to 20 °C (see above). The fraction of fast- and slow-gating channels has previously been estimated from macroscopic current records on the basis of bi-exponential fits to the time course of current decay after channel opening (28, 29). However, we found that this fitting procedure frequently resulted in parameter estimates that were associated with substantial standard errors; also the initial setting of the fit parameters influenced the estimation of the final parameters. To eliminate this potential error source, we introduced a different method to analyze the current decay after channel opening.

Second, the slow-gating mode is characterized by multiple channel reopening during depolarization, which underlies the slowing of macroscopic current decay (27). Hence, the total amount of charge entry should be increased by multiple channel reopening. The integral area between the zero current line and the current decay from the current peak to the current 50 ms after the depolarizing voltage step was used to estimate the amount of total charge entry. Here, big integral values reflect slow current decay as well as a large fraction of slow-gating channels, whereas small integral values reflect rapid current decay and a large fraction of fast-gating channels. Such current-time integrals have previously been used as an indices of the total open channel probability after channel activation (25, 30). To allow a direct comparison of the current-time integrals between single oocytes, the peak of the current traces to be analyzed was always normalized to 1.

Data are expressed as means ± S.E. Statistical comparisons were made using two-tailed Student's *t*-tests. A $p < 0.05$ was considered significant.

RESULTS

Recovery from Ultra-slow Inactivation in μ_1 and DIV-A1529D Channels

Fig. 1A shows the growth of inward currents through wild type μ_1 channels with subsequent 25-ms test pulses at 20-s intervals. From a holding potential of –120 mV, the channels were first inactivated by a 300-s depolarizing prepulse to –50 mV. Recovery from inactivation after returning to –120 mV

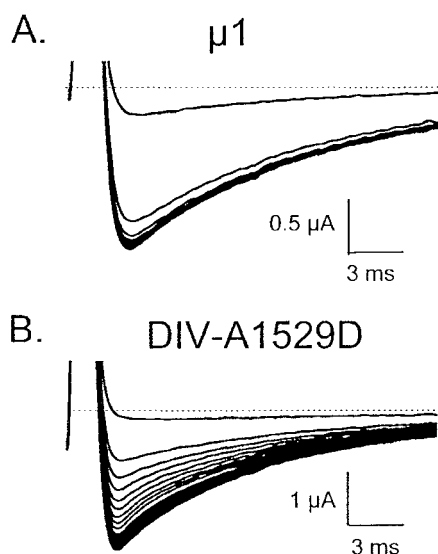


FIG. 1. Ultra-slow inactivation in μ_1 and DIV-A1529D channels. Growth of inward current during recovery from ultra-slow inactivation in wild type μ_1 (A) and mutant DIV-A1529D (B) Na^+ channels expressed in *Xenopus laevis* oocytes. From a holding potential of -120 mV, the channels were inactivated by a 300-s depolarizing step to -50 mV. Thereafter, the potential was returned to -120 mV, and recovery from inactivation was monitored by repetitive 25-ms test pulses to -20 mV at 20-s intervals. The dotted lines indicate the zero current levels. Recovery from ultra-slow inactivation in mutant DIV-A1529D took considerably longer than in μ_1 channels.

was monitored through repetitive test pulses to -20 mV (see “Experimental Procedures”). In wild type μ_1 channels, about 80% of the current recovered within 20 s, whereas the small remaining fraction, about 20%, took several minutes to completely recover (“ultra-slow recovery,” see “Experimental Procedures”).

In contrast to μ_1 channels, mutant DIV-A1529D exhibited a large ultra-slow recovering component of inactivation (Fig. 1B). About 40% of the current recovered within 20 s, whereas the large remaining fraction, about 60%, took several minutes to completely recover.

In a series of such experiments, the calculated fractions of channels recovering from ultra-slow inactivation were 0.22 ± 0.02 ($n = 6$) in μ_1 channels and 0.60 ± 0.02 ($n = 19$) in DIV-A1529D (value for μ_1 taken from Hilber *et al.* (1)). Thus, significantly more channels recovered from ultra-slow inactivation in DIV-A1529D than in μ_1 channels. A more detailed investigation of ultra-slow inactivation in DIV-A1529D channels was carried out in a previous study (1).

Effects of Stabilization of the Fast Inactivated State on Ultra-slow Inactivation in DIV-A1529D Channels

To investigate the relationship between fast inactivation and ultra-slow inactivation, we used different strategies to stabilize the fast inactivated state and tested the effects of these strategies on ultra-slow inactivation.

Stabilization of the Fast Inactivated State by Coexpression of the Rat Brain β_1 Subunit—In wild type μ_1 channels, coexpression of the β_1 subunit stabilizes the fast inactivated state (*e.g.* Refs. 24 and 25). Here, we used coexpression of the β_1 subunit to stabilize the fast inactivated state in DIV-A1529D channels to investigate the effects of fast inactivation on ultra-slow inactivation.

First, we confirmed that the β_1 subunit exhibited similar modulatory effects in DIV-A1529D channels as previously reported for wild type Na^+ channels (22, 23, 31). We compared the current decay in oocytes that were injected either with

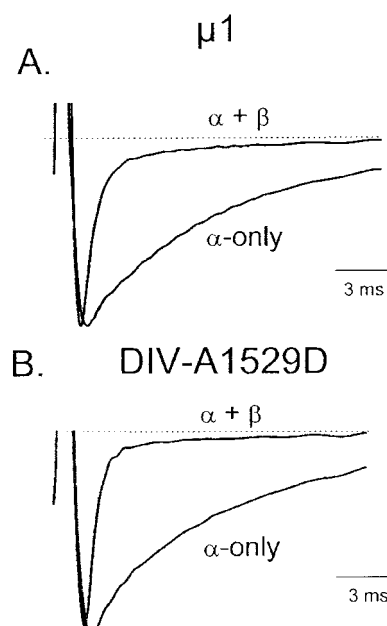


FIG. 2. Current decay with and without coexpression of the rat brain β_1 subunit. Typical examples of original traces of inward currents through wild type μ_1 and $\mu_1 + \beta_1$ (A) channels or mutant DIV-A1529D and DIV-A1529D + β_1 (B) channels elicited by test pulses from -120 to -20 mV. The molar ratio of α/β_1 subunit cRNA injected was ≤ 0.3 . The current amplitudes were normalized to 1. Both in μ_1 and mutant DIV-A1529D channels, coexpression of the β_1 subunit dramatically accelerated the current decay.

DIV-A1529D α -only cRNA or with DIV-A1529D α + rat brain β_1 cRNA (molar α/β_1 ratios ≤ 0.30). Fig. 2A shows typical Na^+ current traces through wild type μ_1 α -only and μ_1 $\alpha + \beta_1$ channels. It can be clearly seen that coexpression of the β_1 subunit substantially accelerated the kinetics of current decay. A similar result was obtained with DIV-A1529D α -only and DIV-A1529D $\alpha + \beta_1$ channels (Fig. 2B). A bi-exponential function (Equation 1) was fit to the decay currents, and the fractions of channels that inactivated with a fast and a slow time constant were calculated (see “Experimental Procedures”). The mean values of time constants (τ_1 , τ_2) and amplitudes (A_1 , A_2) \pm S.E. of a series of such fits are given in Table I. The table shows that both τ_1 and τ_2 were similar in DIV-A1529D α -only and DIV-A1529D + β_1 channels. In contrast, the amplitudes A_1 and A_2 that we used as a measure of the fraction of channels that inactivated with a fast (fast-gating channels) or a slow (slow-gating channels) time constant (see “Experimental Procedures”) were strongly dependent on the coexpression of the β_1 subunit. In DIV-A1529D α -only injected oocytes only a small fraction of channels inactivated with a fast time constant. DIV-A1529D + β_1 channels mainly inactivated with a fast time constant, but in all oocytes investigated, a small but discernable fraction of channels, about 0.07, inactivated with a slow time constant (Table I). Control experiments showed that an α/β_1 ratio of 0.30 was sufficient to obtain a maximum β_1 subunit effect on current decay. There was no significant rise in the fast decay fractions if the β_1 subunit concentration was increased from an α/β_1 ratio of 0.30 to 0.15. An additional increase to 0.07 in three oocytes also showed no effect. The respective fast decay fractions were 0.93 ± 0.01 (α/β_1 ratio, 0.30; $n = 4$), 0.93 ± 0.01 (α/β_1 ratio, 0.15; $n = 4$), and 0.92 ± 0.01 (α/β_1 ratio, 0.07; $n = 3$).

These results show that, as in wild type μ_1 channels (22, 23), coexpression of the β_1 subunit dramatically increased the fraction of fast-gating DIV-A1529D channels, whereas the time constants themselves were not altered. Thus, coexpression of

TABLE I

Parameters of bi-exponential current decay fits Equation 1) of DIV-A1529D α -only and DIV-A1529D $\alpha + \beta_1$ channels expressed in *Xenopus oocytes*

The channels were activated from a holding potential of -120 mV with the voltage step, which elicited maximum current (≈ -20 mV). τ_1 and τ_2 are the time constants of distinct components of recovery; A_1 is the amplitude that was used as a measure of the channel fraction, recovering with the time constant τ_1 (fast fraction). The injected molar cRNA α/β_1 ratio was ≤ 0.3 .

DIV-A1529D		τ_1	τ_2	Fast fraction (A_1)
		(ms)	(ms)	
α -only	Mean	1.2	12.6	0.13
	S.E.	0.2	0.3	0.04
	<i>n</i>	7	14	14
$\alpha + \beta_1$	Mean	1.5	13.5	0.93 ^a
	S.E.	0.1	0.4	0.01
	<i>n</i>	11	11	11

^a Statistically significant difference ($p < 0.01$, unpaired *t* test).

the β_1 subunit exhibits similar effects on the gating properties of DIV-A1529D and μ_1 channels, stabilizing the fast inactivated state in DIV-A1529D channels as well.

Coexpression of the β_1 Subunit Delays Entry to the Ultra-slow Inactivated State in DIV-A1529D Channels—In a previous study (1) we investigated the effects of coexpression of the rat brain β_1 subunit on ultra-slow inactivation in DIV-A1529D channels. We found that the β_1 subunit delayed entry to the ultra-slow inactivated state but did not alter entry voltage dependence.

Fig. 3 shows the recovery of inward currents through DIV-A1529D + β_1 channels with subsequent pulses at 20-s intervals after being inactivated by a 300-s (A) or a 1200-s (B) depolarizing prepulse to -50 mV. We found that the longer prepulse duration substantially delayed recovery from ultra-slow inactivation in DIV-A1529D + β_1 channels. A summary of the recovery curves of four such experiments is shown in the inset. Bi-exponential curve fits to the data points (solid lines) were used to estimate the fraction of DIV-A1529D + β_1 channels, which had entered the ultra-slow inactivated state (see “Experimental Procedures”). This fraction was 0.37 ± 0.03 after a 300-s prepulse and 0.58 ± 0.03 after a 1200-s prepulse to -50 mV ($n = 4$). These fractions were statistically different (paired Student’s *t* test). In DIV-A1529D α -only channels, the corresponding fraction after a 300-s prepulse to -50 mV was 0.60 ± 0.02 ($n = 19$); this fraction was not further increased when longer prepulse durations were used (see Ref. 1). These data confirm that the β_1 subunit prolongs entry to the ultra-slow inactivated state in DIV-A1529D channels.

The use of prepulse durations of >300 s led to unacceptably long experimental durations. Thus, for further experiments, to avoid extremely long prepulse durations (1200 s), we used the channel fraction recovering from ultra-slow inactivation after a 300-s prepulse to -50 mV as a quantitative measure of the modulation of ultra-slow inactivation by the β_1 subunit.

The β_1 Subunit Effect on Ultra-slow Inactivation in DIV-A1529D Channels Depends on the Molar cRNA α/β_1 Ratio—To explore the relationship between the β_1 -induced stabilization of the fast inactivated state and ultra-slow inactivation in more detail, we compared the amount of ultra-slow inactivation produced by a 300-s prepulse to -50 mV with the fraction of channels that showed a fast current decay after activation (the fast-gating fraction). Here, we consider a large fast-gating fraction to reflect a high degree of stabilization of the fast inactivated state.

Xenopus oocytes were injected either with DIV-A1529D α -only cRNA or with both DIV-A1529D α and β_1 subunit cRNA. To generate various fractions of either fast or slow current decay, the molar concentration of the β_1 subunit cRNA was

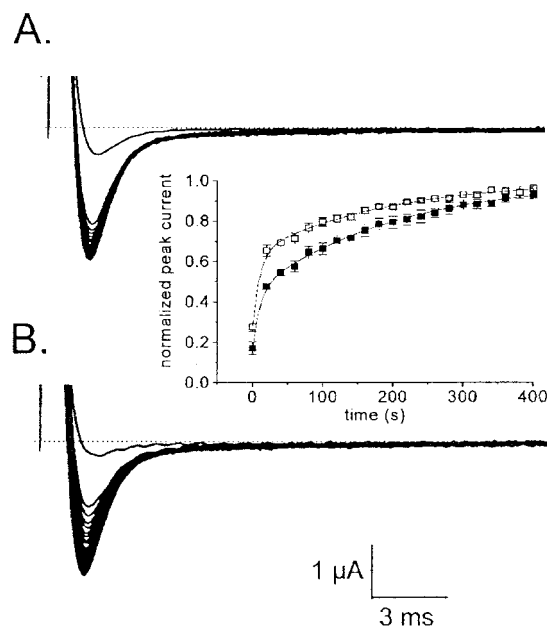


FIG. 3. Coexpression of the β_1 subunit in DIV-A1529D and ultra-slow inactivation. Growth of inward current during recovery from ultra-slow inactivation in DIV-A1529D + β_1 channels after a 300-s (A) or 1200-s (B) depolarizing prepulse to -50 mV (experimental design identical to Fig. 1). The molar ratio of α/β_1 subunit cRNA was ≤ 0.3 . Inset, normalized time course of recovery from inactivation after prepulses to -50 mV for 300-s (open squares, $n = 4$) and for 1200-s (filled squares, $n = 4$).

varied (see “Experimental Procedures”). The lower the cRNA α/β_1 ratio, the greater was the fast-gating channel fraction. In Fig. 4A, the fraction of channels that entered the ultra-slow inactivated state after a 300-s prepulse to -50 mV is plotted against the fraction of channels that showed a fast current decay after activation (see “Experimental Procedures”). Each data point reflects data acquired from experiments on a single oocyte. Fig. 4A shows a linear correlation between the fraction of DIV-A1529D channels exhibiting a fast current decay and the fraction of channels that recovered from ultra-slow inactivation; the larger the fast-gating channel fraction, the smaller was the channel fraction recovering from ultra-slow inactivation. Consequently, stabilization of the fast inactivated state by increasing the β_1 subunit concentration seems to directly inhibit entry to the ultra-slow inactivated state. However, in oocytes showing almost exclusively (93%) fast current decay, a considerable fraction of channels still exhibited ultra-slow inactivation, 0.30 ± 0.02 ($n = 6$). This suggests that ultra-slow inactivation may occur in predominantly fast-mode-gating channels, albeit with a low likelihood.

Fig. 4B shows a similar plot as Fig. 4A, but a different method of analysis of the current decay was used to obtain an additional measure of the extent of stabilization of the fast inactivated state in single oocytes. The fraction of channels that entered the ultra-slow inactivated state after a 300-s prepulse to -50 mV is plotted against the current-time integral (normalized area, see “Experimental Procedures”) after activation by the depolarizing voltage step, which generated maximum current. Similar to Fig. 4A, the plot in Fig. 4B shows a linear correlation between the fraction of fast-gating DIV-A1529D channels (reflected by small current-time integral values) and the fraction of channels that recovered from ultra-slow inactivation; also here, the larger the fraction of fast-gating channels, the smaller was the channel fraction recovering from ultra-slow inactivation. The slightly higher correlation coefficient of the linear regression line given in Fig. 4B compared

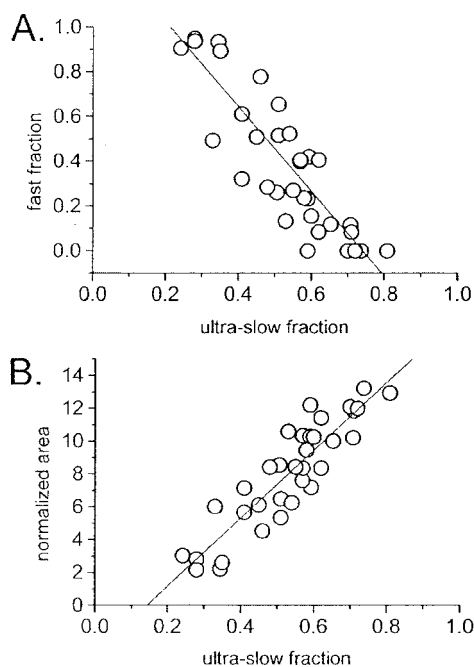


FIG. 4. Current decay and ultra-slow inactivation in DIV-A1529D + β_1 channels. *A*, 50-ms step depolarizations from a holding potential of -120 mV to the voltage that generated maximum inward current were applied to assess current decay after activation. Decay currents were fit by a bi-exponential function. This procedure revealed a large fraction of channels with a fast current decay ($\tau_1 \sim 1$ ms, fast-gating channels) if high concentrations of the β_1 subunit were coexpressed and a large fraction of channels with a slow current decay ($\tau_2 \sim 13$ ms, “slow-gating channels”) in the absence of β_1 , or when low β_1 subunit concentrations were used. Molar α/β_1 ratios from infinite to 0.07 were injected. After assessment of current decay, a 300-s prepulse to -50 mV was applied, and the fraction of channels that recovered from ultra-slow inactivation was estimated as described under “Experimental Procedures.” The fraction of channels recovering from ultra-slow inactivation (x axis) is plotted against the fraction of channels that showed a fast current decay (y axis). Each data point reflects measurements performed on a single oocyte. A linear regression fit to the data points indicated a significant negative correlation between the fast-gating fraction and the propensity to enter the ultra-slow inactivated state ($y = -1.9x + 1.4$, $r = 0.85$, $p < 0.0001$). *B*, same experiments as in *A*, but in this case the fast-gating fraction of channels was estimated from the area under the current trace, reflecting the total amount of charge entry (see “Experimental Procedures”). Oocytes with current-time integrals >10 were considered to reflect channels with a high slow-gating fraction. Linear regression analysis indicated that channels exhibiting a large slow-mode-gating fraction were significantly more susceptible to entry to ultra-slow inactivation than channels with a high fast-mode-gating fraction ($y = -20.6x + 2.9$, $r = 0.9$, $p > 0.0001$).

with that in Fig. 4A might indicate that the use of current-time integrals (see “Experimental Procedures”) to estimate the fast-gating channel fraction is superior to the “curve-fitting method” (see “Experimental Procedures”). However, the results obtained with both methods were reasonably similar (compare Fig. 4, A and B).

The β_1 Subunit Reduces Ultra-slow Inactivation Produced by Trains of Brief Depolarizations in DIV-A1529D Channels—Until now, we have described the effects of β_1 coexpression on ultra-slow inactivation produced by prolonged continuous depolarizations. In a previous study (1), we showed that ultra-slow inactivation could also be produced by brief repetitive depolarizations that enhanced the probability of channels to undergo transitions between closed and open states in DIV-A1529D channels. We concluded that ultra-slow inactivation most likely is attained via transitions from “partially activated” closed states that are accumulated by such pulse trains. Here, we examined whether stabilization of the fast inactivated state by coexpression of the β_1 subunit modulates ultra-slow inactivation

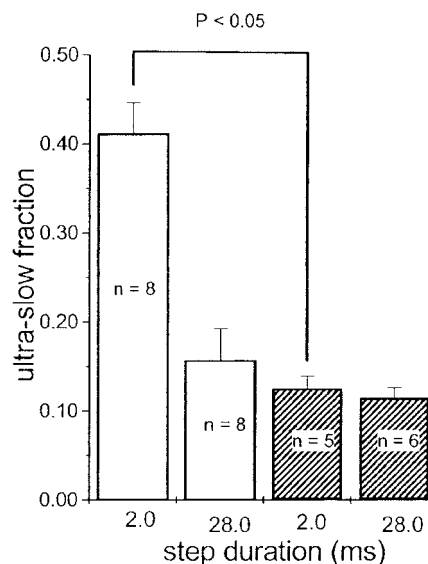


FIG. 5. Coexpression of the β_1 subunit and ultra-slow inactivation elicited by pulse trains. Comparison between the fraction of DIV-A1529D channels (empty bars) recovering from ultra-slow inactivation after a 100-s pulse train, during which repetitive 2-ms step depolarizations to -20 mV were followed by 28-ms periods at -120 mV (30–2-ms train protocol), and after a 100-s pulse train, during which 28-ms step depolarizations to -20 mV were followed by 2-ms periods at -120 mV. The 30–2-ms train forced a considerable channel fraction to enter ultra-slow inactivation. In DIV-A1529D + β_1 channels (hatched bars) (molar ratio of α/β_1 subunit cRNA ≤ 0.3) neither the 30–2- nor the 30–28-ms train protocol elicited considerable ultra-slow inactivation.

generated by pulse trains in a similar way as it modulates ultra-slow inactivation produced by prolonged continuous depolarizations.

Fig. 5 presents a comparison between the fractions of DIV-A1529D channels ($n = 8$) recovering from ultra-slow inactivation after a 100-s pulse train in which repetitive 2-ms step depolarizations to -20 mV were followed by 28-ms periods at -120 mV (30–2-ms train protocol) and after a 100-s pulse train in which 28-ms step depolarizations to -20 mV were followed by 2-ms interpulse intervals at -120 mV (30–28-ms train protocol). During the 30–2-ms train protocol, even though channels spent only 6.7 s at depolarized potentials (-20 mV), a considerable fraction of channels entered the ultra-slow inactivated state (Fig. 5A). This pulse protocol was designed to prevent entry of the channels to the fast inactivated state and to enhance partially activated closed states (1). In contrast, the 30–28-ms train protocol in which the channels spent 93.3 s at depolarized potentials (-20 mV) produced very little ultra-slow inactivation. This pulse protocol most likely enhances fast inactivated states, which accumulate during the 28-ms depolarization periods. These experiments support the notion that enhancement of partially activated closed states favors entry, whereas enhancement of the fast inactivated state reduces entry to the ultra-slow inactivated state.

Coexpression of the β_1 subunit dramatically reduced the fraction of channels that entered the ultra-slow inactivated state after a 30–2-ms train protocol from 0.41 ± 0.04 ($n = 8$) to 0.13 ± 0.01 ($n = 5$). These results suggest that functional association of the β_1 subunit with DIV-A1529D α subunits prevents ultra-slow inactivation produced by pulse train protocols. We propose that the β_1 subunit stabilizes the fast inactivated state during the 30–2-ms train protocol and thereby inhibits ultra-slow inactivation. The time course of current decay of the original current traces shown in Fig. 2B indeed suggests that a considerable fraction of DIV-A1529D $\alpha + \beta_1$ channels entered the fast inactivated state during a 2-ms de-

polarization, whereas in DIV-A1529D α -only channels, this was not the case.

Naturally Occurring Fast Current Decay Reduces Ultra-slow Inactivation in DIV-A1529D α -Only Channels—The observed kinetic effects of β_1 -coexpression are most likely the result of a β_1 -induced shift of equilibria between slow-mode-gating and fast-mode-gating channels. Alternatively, β_1 -coexpression could result in a new kinetic state that is absent in α -only channels. To investigate whether the reduction of ultra-slow inactivation due to the coexpression of the β_1 subunit was caused by stabilization of the “naturally occurring” fast inactivated state as opposed to the induction of a new kinetic state, we compared ultra-slow inactivation in DIV-A1529D α -only-injected oocytes, which naturally exhibited different fast-gating channel fractions. α -Only-injected oocytes normally showed a rather small fast-gating channel fraction (Table I). However, for unknown reasons, a few α -only injected oocytes exhibited a considerable fast-gating channel fraction even though the β_1 subunit was not coexpressed. Such a variation in fast- and slow-gating channel fractions (amplitude ratio of fast to slow component, 0.4–2.9) was also reported for wild type μ_1 channels expressed in oocytes (27).

Current traces recorded from α -only injected oocytes were grouped on the basis of current-time integrals. In general, currents of DIV-A1529D α -only-injected oocytes had current time integrals >10 , which is in excellent agreement with reported data from wild type α -only channels (25). Nevertheless, we were able to find some “outliers,” which, despite the absence of the β_1 subunit, showed current-time integrals <10 . Fig. 6 shows that such α -only channels with current-time integrals <10 , indicating the presence of a large fraction of “naturally” fast-gating channels, had a significantly smaller likelihood of entry to ultra-slow inactivation than α -only channels with current-time integrals >10 . This result suggests that the reduction of ultra-slow inactivation due to the coexpression of the β_1 subunit (see above) is caused by a shift from slow-to fast channel gating by stabilization of the fast inactivated state.

Low Holding Potentials Favor Fast Current Decay and Reduce Ultra-slow Inactivation in DIV-A1529D α -Only Channels—To further explore whether in the absence of the β_1 subunit stabilization of fast inactivation inhibits entry to the ultra-slow inactivated state, we investigated if a slow-to-fast shift in gating forced by a low holding potential (23) also reduces ultra-slow inactivation in DIV-A1529D α -only channels. Therefore, we compared recovery from ultra-slow inactivation in single DIV-A1529D α -only-injected oocytes at two different holding potentials, -120 and -80 mV. Fig. 7 shows the growth of inward current through DIV-A1529D α -only channels with subsequent pulses at 20-s intervals after the channels were first inactivated by a 300-s depolarizing prepulse to -50 mV. In A, the holding and recovery potential was -120 mV; in B it was -80 mV. At -80 mV, the current amplitude was reduced by about 50%. This is due to inactivation of a certain channel fraction that can only be regained when the membrane is hyperpolarized to -120 mV. Moreover, it can be noticed that the current decay was markedly accelerated at -80 mV, indicating that the remaining channel fraction (not inactivated at -80 mV) mainly gated fast. The fraction of channels that recovered from ultra-slow inactivation at a holding potential of -80 mV (0.48 ± 0.04) was significantly reduced (paired t test, $n = 7$) compared with the corresponding fraction at -120 mV (0.61 ± 0.03). These data further confirm that the reduction of ultra-slow inactivation by coexpression of the β_1 subunit in DIV-A1529D channels is caused by a shift from slow to fast channel gating.

Ultra-slow Inactivation Is Inhibited at Potentials That Stabilize the Fast Inactivated State—In a previous study we found

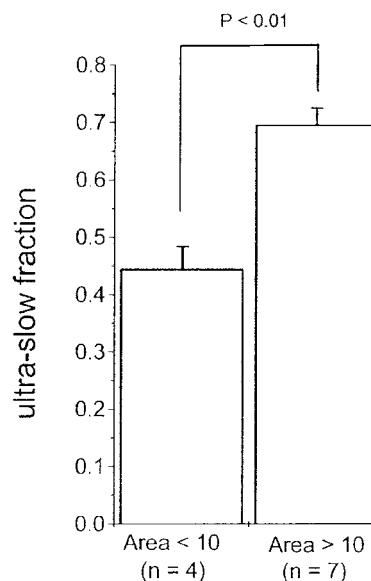


FIG. 6. Current decay and ultra-slow inactivation in DIV-A1529D α -only channels. DIV-A1529D channels were pooled into two groups on the basis of current-time integrals (see Fig. 4B). The current-time integrals of these groups (<10 : 7.1 ± 0.5 , range = 6.0–8.4; >10 : 12.1 ± 0.3 , range = 10.3–13.2) were significantly different ($p < 0.01$). The ordinate indicates the fraction of channels that entered the ultra-slow inactivated state during a 300-s prepulse to -50 mV. DIV-A1529D α -only channels with current-time integrals <10 , i.e. a large fraction of naturally fast-gating channels, had a significantly smaller likelihood of entry to ultra-slow inactivation than α -only channels with current-time integrals >10 .

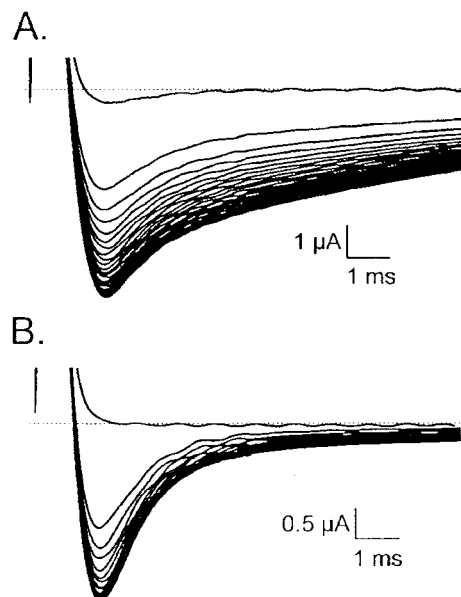


FIG. 7. Ultra-slow inactivation at different holding potentials. Growth of inward current during recovery from ultra-slow inactivation in mutant DIV-A1529D channels at -120 mV (A) and -80 mV (B). From a holding potential of -120 mV or -80 mV, the channels were inactivated by a 300-s depolarizing step to -50 mV. Thereafter, the potential was returned to -120 or -80 mV, and recovery from inactivation was monitored by repetitive test pulses to -20 mV at 20-s intervals. Both current decay and recovery from ultra-slow inactivation were markedly accelerated at the lower holding potential of -80 mV.

that the voltage dependence of ultra-slow inactivation was U-shaped with a local maximum at about -60 mV in DIV-A1529D channels (1). Here, we compared the relationship between the voltage dependence of ultra-slow inactivation and steady-state fast inactivation in DIV-A1529D channels. With

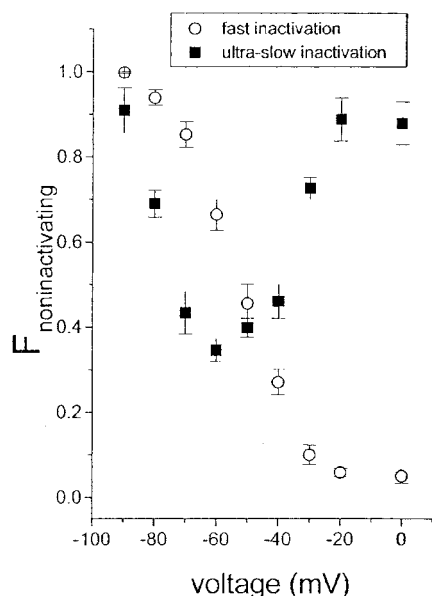


FIG. 8. Voltage dependence of ultra-slow inactivation and steady-state fast inactivation. To assess the voltage dependence of ultra-slow inactivation, the membrane potential was depolarized from -120 mV to the indicated prepulse voltages for 300 s, and the time course of recovery at -120 mV was monitored for each prepulse potential as described under “Experimental Procedures.” The time course of recovery from ultra-slow inactivation was then fit with a bi-exponential function (Equation 1) to estimate the fraction of channels recovering from ultra-slow inactivation (A_2). Channel availability defined as the fraction of channels not recovering from ultra-slow inactivation ($1 - A_2 = F_{\text{noninactivating}}$) is plotted as a function of prepulse voltage (these data are reproduced from Fig. 2 in Ref. 1). Steady-state fast inactivation was assessed by delivery of 20-ms test pulses to -20 mV after 50-ms prepulses to the indicated potentials. The respective test pulse current was normalized to the current under fully available conditions. Each data point reflects the mean of several experiments (n always ≥ 4). Whereas steady-state fast inactivation became more complete at prepulse voltages positive to -60 mV, ultra-slow inactivation reached a local minimum at -60 mV.

this approach, we could directly compare the occupancy of the fast inactivated state with the occupancy of the ultra-slow inactivated state at various voltages. Fig. 8 shows the voltage dependence of ultra-slow inactivation and steady state fast inactivation in DIV-A1529D channels. The plot shows that ultra-slow inactivation already started to occur at weak depolarizing potentials between -90 and -80 mV. A considerable fraction of channels entered the ultra-slow inactivated state (>0.5) at -70 mV, a potential at which hardly any channels ($<15\%$) entered the fast inactivated state during a 50-ms prepulse. When the depolarizing potential was further increased to -60 mV, the fraction of ultra-slow inactivated channels reached a local maximum. At this potential, fast inactivation started to occur more prominently, *i.e.* more than 30% of the channels entered the fast inactivated state during a 50-ms prepulse. As the depolarizing potential was further increased from -50 to 0 mV, the fast inactivated state was increasingly stabilized. At the same time, entry to the ultra-slow inactivated state was inhibited with increasing depolarization, reaching a minimum at potentials where almost 100% fast inactivation occurred. These experiments strongly suggest that stabilization of the fast inactivated state directly inhibits the transition to the ultra-slow inactivated state in DIV-A1529D channels.

Effects of Destabilization of the Fast Inactivated State on Ultra-slow Inactivation in DIV-A1529D Channels

The Inactivation-defective DIV-A1529D Channel Mutant I1303Q/F1304Q/M1305Q Enhances Ultra-slow Inactivation—

The strategy of all the experiments presented above was based on the stabilization of the fast inactivated state by different methods. We found that stabilization of the fast inactivated state inhibited ultra-slow inactivation. Consequently, destabilization of the fast inactivated state should enhance ultra-slow inactivation. Fast inactivation can be destabilized by mutations in the I¹³⁰³F¹³⁰⁴M¹³⁰⁵ motif, which is located on the linker between DIII and DIV of the μ_1 Na⁺ channel (3, 4, 32). Fig. 9 shows the growth of inward currents through inactivation-defective DIV-A1529D + I1303Q/F1304Q/M1305Q channels with subsequent pulses at 20-s intervals. From a holding potential of -120 mV, the channels were first inactivated by a 300-s depolarizing prepulse to -50 mV (A) or -20 mV (B). Recovery from inactivation after returning to -120 mV was monitored through repetitive test pulses to -20 mV. In both cases, a considerable fraction of channels recovered with a very slow time constant on the order of ~ 100 s.

The summaries of the recovery curves of a series of such experiments are shown in Fig. 9C. Bi-exponential curve fits to the data points (*solid lines*, see “Experimental Procedures”) were used to estimate the fraction of DIV-A1529D + I1303Q/F1304Q/M1305Q channels that had entered the ultra-slow inactivated state after a 300-s prepulse to -50 and -20 mV. These fractions were 0.58 ± 0.01 ($n = 12$) and 0.44 ± 0.01 ($n = 5$), respectively. In DIV-A1529D channels that were not inactivation-defective, the corresponding fractions were 0.60 ± 0.02 ($n = 19$) and 0.13 ± 0.02 ($n = 7$). Comparing these fractions between inactivation-defective DIV-A1529D + I1303Q/F1304Q/M1305Q channels and DIV-A1529D channels, it can be noticed that a prepulse potential of -50 mV produced similar fractions of channels recovering from ultra-slow inactivation in both cases, whereas a prepulse potential of -20 mV produced considerable ultra-slow inactivation only in inactivation-defective channels. Also shown in Fig. 9C is the time course of recovery from a 300-s inactivating prepulse to -20 mV in I1303Q/F1304Q/M1305Q channels that did not carry the additional DIV-A1529D mutation in the selectivity filter ($n = 7$). In these channels recovery assumed a mono-exponential time course (Equation 2) with a time constant of ~ 30 s, which is in good agreement with previously reported findings (17). The state from which channels recover with a time constant of ~ 30 s has been referred to as “slow” inactivation. The fact that adding the “selectivity filter mutation” DIV-A1529D to the “inactivation gate mutation” I1303Q/F1304Q/M1305Q changes the mono-exponential time course of recovery from non-fast inactivation in I1303Q/F1304Q/M1305Q to a bi-exponential time course in DIV-A1529D + I1303Q/F1304Q/M1305Q suggests that the mutation DIV-A1529D created an additional inactivated state, *i.e.* ultra-slow inactivation. These results support the notion that the ultra-slow inactivated state observed in some selectivity filter mutations (1, 16) is distinct from the enhanced slow inactivated state observed in inactivation-defective channels (17, 20, 33, 34).

Stabilization of the fast inactivated state by a strongly depolarized potential (-20 mV) dramatically inhibits entry to the ultra-slow inactivated state in DIV-A1529D channels but not in inactivation-defective DIV-A1529D + I1303Q/F1304Q/M1305Q channels (Fig. 9C). In the latter, the fast inactivated state cannot be efficiently stabilized due to the mutations I1303Q/F1304Q/M1305Q.

If the fast inactivated state cannot be stabilized in inactivation-defective DIV-A1529D + I1303Q/F1304Q/M1305Q channels, coexpression of the β_1 subunit, which stabilizes the fast inactivated state in DIV-A1529D channels should not affect the fraction of DIV-A1529D + I1303Q/F1304Q/M1305Q channels

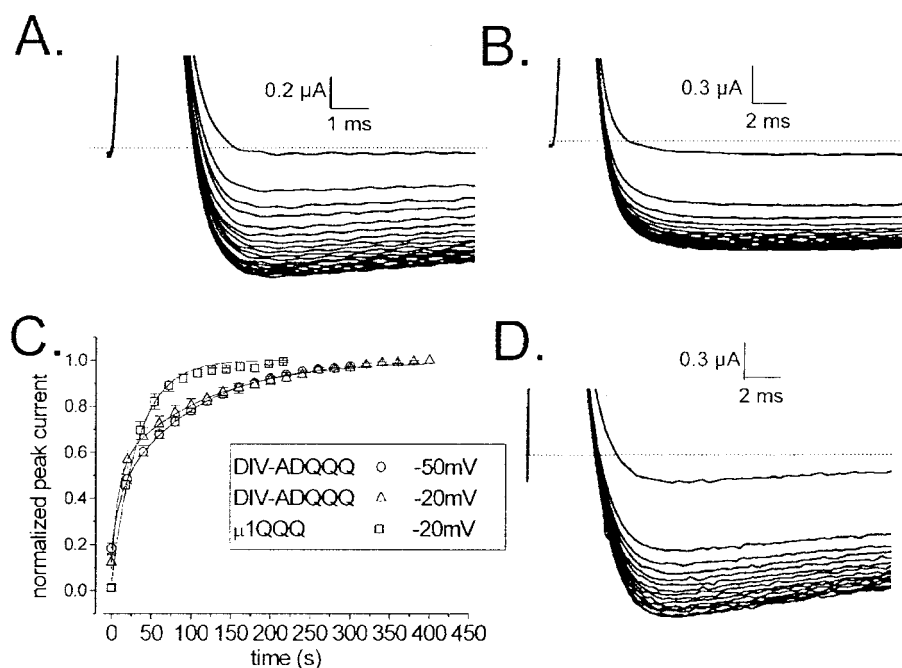


FIG. 9. Ultra-slow inactivation in inactivation-defective DIV-A1529D + I1303Q/F1304Q/M1305Q channels. *A*, growth of inward current during recovery from ultra-slow inactivation in DIV-A1529D + I1303Q/F1304Q/M1305Q. From a holding potential of -120 mV, the channels were inactivated by a 300-s depolarizing step to -50 mV. Thereafter, the potential was returned to -120 mV, and recovery from inactivation was monitored by repetitive test pulses to -20 mV at 20-s intervals. *B*, like *A*, but a 300-s depolarizing step to -20 mV was applied. *C*, comparison of the time courses of recovery from inactivation obtained from a series of such experiments after 300-s prepulses to -50 mV ($n = 12$) or to -20 mV ($n = 5$). Peak inward currents were normalized to the final current level attained after full recovery. Recovery from ultra-slow inactivation took slightly longer after 300-s prepulses to -50 mV. For comparison, recovery from 300-s prepulses to -20 mV in the single mutant μ_1 -I1303Q/F1304Q/M1305Q is shown ($n = 7$). Whereas the time course of recovery in DIV-A1529D + I1303Q/F1304Q/M1305Q (DIV-ADQQQ) was best fit by a bi-exponential equation (Equation 1), the time course of recovery in μ_1 -I1303Q/F1304Q/M1305Q was best fit by a mono-exponential function (Equation 2). *D*, growth of inward current during recovery from ultra-slow inactivation in DIV-A1529D + I1303Q/F1304Q/M1305Q + β_1 channels. From a holding potential of -120 mV, the channels were inactivated by a 300-s depolarizing step to -20 mV. Thereafter, the recovery from ultra-slow inactivation was similar to DIV-A1529D + I1303Q/F1304Q/M1305Q α -only channels (compare with *B*). Functional association of the β_1 subunit with inactivation-defective DIV-A1529D α subunits is confirmed by the acceleration of the current decay (compare with *B*).

that can be driven to the ultra-slow inactivated state. Fig. 9*D* shows the growth of inward currents through DIV-A1529D + I1303Q/F1304Q/M1305Q + β_1 channels with subsequent pulses at 20-s intervals. The experimental conditions were identical to those in Fig. 9*B*. The accelerated current decay in Fig. 9*D* compared with 9*B* suggests functional coexpression of the β_1 subunit. The fraction of inactivation-defective $\alpha + \beta_1$ channels recovering from ultra-slow inactivation after a 300-s prepulse to -20 mV, 0.43 ± 0.01 ($n = 4$), was very similar to the corresponding fraction of α -only channels, 0.44 ± 0.01 ($n = 5$). Hence, coexpression of the β_1 subunit with DIV-A1529D + I1303Q/F1304Q/M1305Q channels did not affect ultra-slow inactivation.

DISCUSSION

In this study, we investigated the relationship between fast inactivation and ultra-slow inactivation in DIV-A1529D channels. We recently reported that ultra-slow inactivation, which is characterized by time constants of entry to and recovery from inactivation in the order of ~ 100 s, is enhanced by charge-altering mutations of residues DIII-K1237 and DIV-A1529. Both residues are located in the putative selectivity filter of the channel. Entry to the ultra-slow inactivated state could be reduced by binding to the outer pore of a mutant μ -CTX, suggesting that ultra-slow inactivation may reflect a structural rearrangement of the outer vestibule (1, 16).

First evidence in support for the existence of coupling between fast and ultra-slow inactivation came from experiments where we coexpressed the rat brain β_1 subunit with DIV-A1529D channels in *Xenopus* oocytes. We found that coexpres-

sion of the β_1 subunit significantly delayed entry of DIV-A1529D channels to the ultra-slow inactivated state during prolonged depolarizations (1).

The β_1 Subunit Delays Entry to Ultra-slow Inactivation via Stabilization of the Fast Inactivated State—In wild type μ_1 channels, functional association of the β_1 subunit with the α subunit stabilizes the fast inactivated state (e.g. Refs. 24 and 25). In the presence of β_1 , the fast-gating mode is favored over the slow-gating mode, resulting in a dramatic acceleration of the current decay after channel activation (22, 23).

In this study, we showed that coexpression of the β_1 subunit exhibited similar modulatory effects on the current decay of DIV-A1529D and wild type μ_1 channels (Fig. 2). The β_1 effects on DIV-A1529D channels (Table I) compare well with those of previous reports on μ_1 channels (22, 23). This indicates that the functional association of β_1 with the α subunit was not disturbed by introducing the mutation DIV-A1529D. Thus, coexpression of the β_1 subunit does, as in μ_1 channels, stabilize the fast inactivated state in DIV-A1529D channels.

As shown in Fig. 3, coexpression of the β_1 subunit delayed entry to the ultra-slow inactivated state during prolonged depolarizations in DIV-A1529D channels. This was also shown in a previous study (1). Coexpression of the β_1 subunit also significantly inhibited ultra-slow inactivation produced by trains of brief depolarizations (Fig. 5). Such pulse trains may resemble physiological conditions (i.e. continuous action potential firing in neurons or muscle cells) more closely than prolonged continuous depolarizations. The inhibition of ultra-slow inactivation by the β_1 subunit in DIV-A1529D channels was directly

related to the stabilization of the fast inactivated state since a negative linear correlation was found between the fraction of channels exhibiting a fast current decay and the fraction of channels that recovered from ultra-slow inactivation (Fig. 4).

The notion that the reduction of ultra-slow inactivation by β_1 occurs via stabilization of the fast inactivated state gains further support by the observation that ultra-slow inactivation evoked by frequent depolarizations was suppressed by β_1 to a significantly higher degree than ultra-slow inactivation evoked by prolonged depolarizations. As shown in Fig. 5, in the absence of β_1 , repetitive short (2 ms) depolarizations drove more channels into ultra-slow inactivation than repetitive long (28-ms) depolarizations. During the 2-ms depolarizations only a small number of channels might have entered the fast inactivated state, resulting in a high likelihood of entry to ultra-slow inactivation. The presence of β_1 allows more fast inactivation to occur even during such short 2-ms depolarizations (compare current decays in Fig. 2) with the consequence of a smaller fraction of channels entering the ultra-slow inactivated state.

It might be argued that the reduction of ultra-slow inactivation by β_1 does not result from a shift from slow-to-fast mode channel-gating but may be caused by the induction of a new kinetic state. In this case, β_1 -independent slow-to-fast mode shifts should have no effect on the number of channels entering ultra-slow inactivation. Shifts from slow-to-fast-gating mode are known to occur in the absence of β_1 , albeit at a slower rate than in the presence of β_1 (23). Thus, we wondered whether those DIV-A1529D-injected oocytes that in the absence of β_1 showed a high amount of fast current decay also exhibited less ultra-slow inactivation than oocytes showing almost exclusively slow current decay. Fig. 6 demonstrates that α -only-injected oocytes that were selected for fast current decay indeed showed substantially less ultra-slow inactivation. Furthermore, low holding potentials, which favor fast current decay (23) by eliminating the slow-gating channel fraction, significantly inhibited ultra-slow inactivation (Fig. 7). Finally, increasing stabilization of fast inactivation with stronger depolarizations reduced entry to ultra-slow inactivation (Fig. 8).

If stabilization of the fast inactivated state inhibits ultra-slow inactivation in DIV-A1529D channels, destabilization of the fast inactivated state would be expected to enhance ultra-slow inactivation. To destabilize the fast inactivated state, we used DIV-A1529D channels with the additional mutations I1303Q/F1304Q/M1305Q, which selectively remove fast inactivation (3, 4, 32). Indeed, a considerable fraction of fast inactivation-defective DIV-A1529D + I1303Q/F1304Q/M1305Q channels could be driven to the ultra-slow inactivated state during a 300-s depolarization to -20 mV (Fig. 9). At this voltage, hardly any DIV-A1529D channels with normal fast inactivation properties entered the ultra-slow inactivated state most probably because they were fast inactivated.

Nevertheless, the fraction of DIV-A1529D + I1303Q/F1304Q/M1305Q channels that entered the ultra-slow inactivated state after a 300-s prepulse to -20 mV, ~ 0.44 , was significantly smaller than the corresponding fraction after a 300-s prepulse to -50 mV, ~ 0.58 . This indicated that stronger depolarizations modestly inhibited entry to the ultra-slow inactivated state also in fast inactivation-defective DIV-A1529D + I1303Q/F1304Q/M1305Q channels.

Less ultra-slow inactivation at more positive potentials suggests a non-monotonic voltage dependence. In Hilber *et al.* (1) we proposed that such a non-monotonic voltage dependence of ultra-slow inactivation in DIV-A1529D channels may arise if ultra-slow inactivation is reached via transitions from partially activated closed states that are passed through on the way up to the open state during activation. This hypothesis was sup-

ported by the fact that the voltage dependence of ultra-slow inactivation was U-shaped with a local maximum of inactivation at around -50 to -60 mV (1), *i.e.* within a voltage range that has a high probability to accumulate intermediate closed states. Entry to the ultra-slow inactivated state from intermediate closed states is further corroborated by the fact that a considerable fraction of DIV-A1529D channels could be driven into ultra-slow inactivation by trains of brief depolarizations (Fig. 5), which were designed to accumulate partially activated closed states and to avoid fast inactivated states (1, 35). The fact that the fast inactivation-defective DIV-A1529D + I1303Q/F1304Q/M1305Q channels still exhibited a “residual” U-shaped voltage dependence of ultra-slow inactivation supports the notion that ultra-slow inactivation in this mutant is reached via transitions from pre-open states.

Whereas coexpression of the β_1 subunit significantly reduced ultra-slow inactivation in DIV-A1529D channels, ultra-slow inactivation was not affected by β_1 in inactivation-defective DIV-A1529D + I1303Q/F1304Q/M1305Q channels (Fig. 9). The lack of modulation of ultra-slow inactivation by β_1 in inactivation-defective channels does not seem to result from “uncoupling” of β_1 from the α -subunit as functional association of β_1 with fast inactivation-defective channel mutants was previously reported (33). Accordingly, in our experiments we observed an accelerated current decay in DIV-A1529D + I1303Q/F1304Q/M1305Q + β_1 channels (compare current traces of Fig. 9, B and D), indicating that β_1 still exerted a modulatory effect on inactivation-defective channels. However, the defect in fast inactivation obviously resulted in a complete loss of β_1 subunit modulation of ultra-slow inactivation. Hence, β_1 needs functional fast inactivation to be able to modulate ultra-slow inactivation in DIV-A1529D channels.

Relationship between Slow and Ultra-slow Inactivation—If μ_1 Na⁺ channels are inactivated for up to 60 s, they recover with a time constant of about 30 s (17). The state from which μ_1 channels recover with a time constant of several seconds has been termed slow inactivation (36). If μ_1 channels are inactivated for substantially longer periods, *i.e.* 5–10 min, recovery exhibits a bi-exponential time course with a slow time constant of ~ 10 s and an additional ultra slow time constant of ~ 100 s (1, 16, 37). Selective removal of fast inactivation by the mutation I1303Q/F1304Q/M1305Q allows slow inactivation to occur more quickly and completely (17, 33). A similar enhancement of slow inactivation by disruption of fast inactivation has been demonstrated in human skeletal muscle Na⁺ channels (34) and human cardiac Na⁺ channels (20). An interaction between fast and slow inactivation has also been found in rat brain IIA Na⁺ channels (38). As shown in the present study, defective fast inactivation not only enhances slow inactivation but also produces more ultra-slow inactivation (Fig. 9).

The fact that disabling of fast inactivation increases the likelihood of both slow and ultra-slow inactivation raises the question of whether slow and ultra-slow inactivation are tightly coupled processes. For the following reasons we believe that the ultra-slow inactivated state is distinct from slow inactivation and that direct transitions between these states are unlikely.

First, the addition of the selectivity filter mutation DIV-A1529D to the inactivation gate mutation I1303Q/F1304Q/M1305Q changed the mono-exponential time course of recovery from non-fast inactivation in I1303Q/F1304Q/M1305Q to a bi-exponential time course in DIV-A1529D + I1303Q/F1304Q/M1305Q (Fig. 9C). This suggests that the mutation DIV-A1529D created an additional inactivated state, *i.e.* ultra-slow inactivation.

Second, as shown in a previous study, slow inactivation

produced by 1-s prepulses in mutant DIV-A1529D had a monotonic voltage dependence, whereas the voltage dependence of ultra-slow inactivation was U-shaped, again arguing against direct transitions between slow inactivation and ultra-slow inactivation (1).

Possible Molecular Mechanisms of the Inhibition of Ultra-slow Inactivation by Fast Inactivation—Fast inactivation has been shown to immobilize gating charge (21). The voltage sensor (S4 segment) in DIV of the Na⁺ channel α subunit appears to have a unique role in the voltage control of inactivation (38–41) and is most likely to be immobilized during manifestation of the fast inactivated state (42–44) (“voltage sensor trapping”). If slower forms of inactivation depend on the mobility of one or more S4 segments, then S4 immobilization by fast inactivation may limit entry to slower forms of inactivation (17, 20). In the case of ultra-slow inactivation it is noteworthy that the voltage sensor likely to control inactivation and the residue that controls ultra-slow inactivation (alanine 1529) are both located in DIV.

On the other hand, such a “competition” for gating charge immobilization among different inactivated states would imply that fast and slow forms of inactivation are tightly coupled. Other authors recently demonstrated that neither the equilibrium of fast- and non-fast inactivated channels nor the kinetics of recovery from fast inactivation are altered by the closure of the slow gate (18). Thus, fast and non-fast inactivation are only weakly coupled, which argues against the notion that fast inactivation limits the amount of slow inactivation by gating charge immobilization.

Aside from “competition for voltage-sensor trapping,” fast inactivation may interact with ultra-slow inactivation via conformational changes that are elicited by binding of the inactivation particle to its docking site. According to the prevailing molecular model, the Na⁺ channel pore is surrounded by the S6 segments of all four domains (45). The S6 segment in DIV appears to play a significant role both in fast inactivation (4, 46–49) and in slow inactivation (7, 49, 50). The intracellular end of DIV-S6 has been proposed to serve as receptor for the inactivation gate (4). However, not the IFM motif itself, but an unidentified motif in the inactivation gate may bind to critical amino acid residues in DIV-S6 (46). We suggest that binding of the inactivation particle to a receptor at the cytoplasmic end of DIV-S6 could induce a conformational change in this transmembrane segment, which is then transmitted to the DIV-P-loop, resulting in an interaction between fast and ultra-slow inactivation. Thus, the conformational change of the outer vestibule, which is mirrored by ultra-slow inactivation, may be modulated allosterically via binding of the inactivation particle to its receptor.

Alternatively ultra-slow inactivation may reflect a molecular rearrangement that is not confined to the outer vestibule but involves both the extracellular and the cytoplasmic pore. In this case, binding of the inactivation gate to its receptor might stabilize the channel structure and thereby inhibit ultra-slow inactivation. This idea has its precedent in the interaction of μ -CTX with the outer channel vestibule; we recently reported that superfusion with a mutant μ -CTX reduced entry to the ultra-slow inactivated state (1, 16). This toxin is believed to bind to the outer vestibule of the Na⁺ channel. However, the block of the outer channel pore is incomplete, resulting in the flow of residual current, which allows the examination of channel gating in the blocked state (16, 51, 52). The reduction of entry to the ultra-slow inactivated state by the mutant μ -CTX R13Q led us to propose that ultra-slow inactivation most likely reflects a rearrangement of the outer pore region and that binding of the mutant μ -CTX to the outer pore stabilizes the

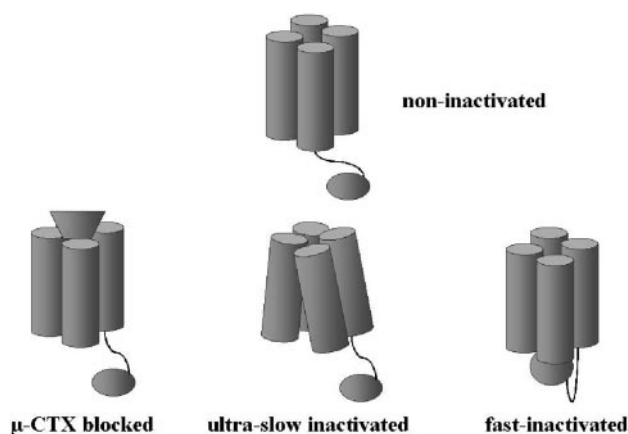


FIG. 10. **Proposed mechanism of protection from ultra-slow inactivation by fast inactivation.** Schematic depicting a hypothetical mechanism underlying the protection from ultra-slow inactivation by the fast inactivated state. Shown are the four domains surrounding the central channel pore and the inactivation ball tethered to the channel. We hypothesize that the ultra-slow inactivated state represents a complex structural rearrangement of the channel structure (*ultra-slow inactivated*). Channels can be protected from entry to the ultra-slow inactivated state by binding to the outer vestibule of a mutant μ -CTX, which presumably stabilizes the channel structure (*μ -CTX blocked*). Likewise, binding of the fast-inactivation ball to the cytoplasmic pore might stabilize the channel structure and thereby reduce the fraction of channels susceptible to entry to the ultra-slow inactivated state.

structure of the outer vestibule, thereby protecting channels from ultra-slow inactivation. By analogy, binding of the inactivation particle to its receptor at the cytoplasmic pore might as well stabilize the channel structure and interfere with ultra-slow inactivation, provided that ultra-slow inactivation represents a broad molecular rearrangement of the channel molecule (Fig. 10).

Physiologic Significance of Ultra-slow Inactivation—Various forms of prolonged inactivation may be of substantial significance in a broad variety of physiological and pathological settings. In neurons, accumulation of Na⁺ channel-prolonged inactivation may influence activity-dependent neuronal excitability, especially under pathological conditions of intense discharge such as epilepsy (53). Specifically, some forms of generalized epilepsy with febrile seizures are associated with a mutation in the Na⁺ channel β_1 subunit (14). This underscores the clinical relevance of β_1 -induced modulation of Na⁺ channel function. In skeletal muscle, differences in Na⁺ channel-prolonged inactivation may underlie differences in fast- and slow-twitch muscle excitability (54). Several genetic skeletal muscle diseases are the result of defects in inactivation (reviewed in Ref. 5). In the heart, myocardial infarction has been shown to result in a delay in recovery from inactivation of Na⁺ currents (55, 56). This effect may produce inhomogeneities of cardiac impulse conduction and set the stage for reentrant arrhythmias and, ultimately, predispose to sudden cardiac death. It is evident that understanding the mechanisms of prolonged inactivation will enable the definition of new targets for drug development and may lead to therapeutic strategies against neurologic, neuromuscular, and cardiac disorders.

Recently, a bacterial voltage-gated Na⁺ channel has been expressed and characterized (57). This channel is a homotetramer, and each α -subunit contains six transmembrane segments. The selectivity filter of this channel is predicted to contain four glutamates, whereas the mammalian Na⁺ channel selectivity filter contains the motif DEKA (58). Despite the absence of an obvious inactivation particle, the bacterial Na⁺ channel inactivates, albeit at a much slower rate than its

mammalian counterpart. We have demonstrated that if the DEKA motif of the mammalian Na⁺ channel is converted into either DEEA (16) or DEKD (1) an inactivated state that occurs by closure of the external channel mouth is produced. Thus, the bacterial one-domain Na⁺ channel may represent a physiologic counterpart to the mutants, which exhibit ultra-slow inactivation.

Acknowledgments—We thank Yu Huang, Bei Li, Gayle Tonkovich, and Anton Karel for technical assistance. Martin Horvath and Evelyne Gross are acknowledged for animal care.

REFERENCES

- Hilber, K., Sandtner, W., Kudlacek, O., Glaaser, I. W., Weisz, E., Kyle, J. W., French, R. J., Fozzard, H. A., Dudley, S. C., and Todt, H. (2001) *J. Biol. Chem.* **276**, 27831–27839
- Hilber, K., Sandtner, W., Kudlacek, O., Singer, E., and Todt, H. (2002) *Soc. Neurosci. Abstr.* **27**, No. 46.12
- West, J. W., Patton, D. E., Scheuer, T., Wang, Y., Goldin, A. L., and Catterall, W. A. (1992) *Proc. Natl. Acad. Sci. U. S. A.* **89**, 10910–10914
- McPhee, J. C., Ragsdale, D. S., Scheuer, T., and Catterall, W. A. (1994) *Proc. Natl. Acad. Sci. U. S. A.* **91**, 12346–12350
- Cannon, S. C. (1996) *Trends Neurosci.* **19**, 3–10
- Cummins, T. R., and Sigworth, F. J. (1996) *Biophys. J.* **71**, 227–236
- Hayward, L. J., Brown, R. H., Jr., and Cannon, S. C. (1997) *Biophys. J.* **72**, 1204–1219
- Hayward, L. J., Sandoval, G. M., and Cannon, S. C. (1999) *Neurology* **52**, 1447–1453
- Bendahou, S., Cummins, T. R., Hahn, A. F., Langlois, S., Waxman, S. G., and Ptacek, L. J. (2000) *J. Clin. Invest.* **106**, 431–438
- Struyk, A. F., Scoggan, K. A., Bulman, D. E., and Cannon, S. C. (2000) *J. Neurosci.* **20**, 8610–8617
- Wang, Q., Shen, J., Splawski, I., Atkinson, D., Li, Z., Robinson, J. L., Moss, A. J., Towbin, J. A., and Keating, M. T. (1995) *Cell* **80**, 805–811
- Bennett, P. B., Yazawa, K., Makita, N., and George, A. L. J. (1995) *Nature* **376**, 683–685
- Dumaine, R., Wang, Q., Keating, M. T., Hartmann, H. A., Schwartz, P. J., Brown, A. M., and Kirsch, G. E. (1996) *Circ. Res.* **78**, 916–924
- Wallace, R. H., Wang, D. W., Singh, R., Scheffer, I. E., George, A. L., Jr., Phillips, H. A., Saar, K., Reis, A., Johnson, E. W., Sutherland, G. R., Berkovic, S. F., and Mulley, J. C. (1998) *Nat. Genet.* **19**, 366–370
- Bendahou, S., Cummins, T. R., Griggs, R. C., Fu, Y. H., and Ptacek, L. J. (2001) *Ann. Neurol.* **50**, 417–420
- Todt, H., Dudley, S. C. J., Kyle, J. W., French, R. J., and Fozzard, H. A. (1999) *Biophys. J.* **76**, 1335–1345
- Featherstone, D. E., Richmond, J. E., and Ruben, P. C. (1996) *Biophys. J.* **71**, 3098–3109
- Vedantham, V., and Cannon, S. C. (1998) *J. Gen. Physiol.* **111**, 83–93
- Rudy, B. (1978) *J. Physiol. (Lond.)* **283**, 1–21
- Richmond, J. E., Featherstone, D. E., Hartmann, H. A., and Ruben, P. C. (1998) *Biophys. J.* **74**, 2945–2952
- Armstrong, C. M., and Bezanilla, F. (1977) *J. Gen. Physiol.* **70**, 567–590
- Patton, D. E., Isom, L. L., Catterall, W. A., and Goldin, A. L. (1994) *J. Biol. Chem.* **269**, 17649–17655
- Chang, S. Y., Satin, J., and Fozzard, H. A. (1996) *Biophys. J.* **70**, 2581–2592
- Schreibmayer, W., Frohnwieser, B., Dascal, N., Platzter, D., Spreitzer, B., Zechner, R., Kallen, R. G., and Lester, H. A. (1994) *Receptors Channels* **2**, 339–350
- Balsler, J. R., Nuss, H. B., Romashko, D. N., Marban, E., and Tomaselli, G. F. (1996) *J. Gen. Physiol.* **107**, 643–658
- Patlak, J. B., and Ortiz, M. (1986) *J. Gen. Physiol.* **87**, 305–326
- Zhou, J. Y., Potts, J. F., Trimmer, J. S., Agnew, W. S., and Sigworth, F. J. (1991) *Neuron* **7**, 775–785
- Cannon, S. C., McClatchey, A. I., and Gusella, J. F. (1993) *Pfluegers Arch. Eur. J. Physiol.* **423**, 155–157
- Stevens, E. B., Cox, P. J., Shah, B. S., Dixon, A. K., Richardson, P. J., Pinnoch, R. D., and Lee, K. (2001) *Pfluegers Arch. Eur. J. Physiol.* **441**, 481–488
- Wang, D. W., Nie, L., George, A. L. J., and Bennett, P. B. (1996) *Biophys. J.* **70**, 1700–1708
- Isom, L. L., De Jongh, K. S., Patton, D. E., Reber, B. F., Offord, J., Charbonneau, H., Walsh, K., Goldin, A. L., and Catterall, W. A. (1992) *Science* **256**, 839–842
- Agnew, W. S., Cooper, E. C., Shenkel, S., Correa, A. M., James, W. M., Ukomadu, C., and Tomiko, S. A. (1991) *Ann. N. Y. Acad. Sci.* **625**, 200–223
- Nuss, H. B., Balsler, J. R., Orias, D. W., Lawrence, J. H., Tomaselli, G. F., and Marban, E. (1996) *J. Physiol. (Lond.)* **494**, 411–429
- Alekov, A. K., Peter, W., Mitrovic, N., Lehmann-Horn, F., and Lerche, H. (2001) *Neurosci. Lett.* **306**, 173–176
- Aldrich, R. W. (1981) *Biophys. J.* **36**, 519–532
- Balsler, J. R., Nuss, H. B., Chiamvimonvat, N., Perez-Garcia, M. T., Marban, E., and Tomaselli, G. F. (1996) *J. Physiol. (Lond.)* **494**, 431–442
- Fox, J. M. (1976) *Biochim. Biophys. Acta* **426**, 232–244
- Kontis, K. J., and Goldin, A. L. (1997) *J. Gen. Physiol.* **110**, 403–413
- Chahine, M., George, A. L., Jr., Zhou, M., Ji, S., Sun, W., Barchi, R. L., and Horn, R. (1994) *Neuron* **12**, 281–294
- Chen, L. Q., Santarelli, V., Horn, R., and Kallen, R. G. (1996) *J. Gen. Physiol.* **108**, 549–556
- Mitrovic, N., George, A. L., and Horn, R. (2000) *J. Gen. Physiol.* **115**, 707–718
- Cha, A., Ruben, P. C., George, A. L. J., Fujimoto, E., and Bezanilla, F. (1999) *Neuron* **22**, 73–87
- Kuhn, F. J., and Greeff, N. G. (1999) *J. Gen. Physiol.* **114**, 167–183
- Sheets, M. F., Kyle, J. W., and Hanck, D. A. (2000) *J. Gen. Physiol.* **115**, 609–620
- Fozzard, H. A., and Hanck, D. A. (1996) *Physiol. Rev.* **76**, 887–926
- McPhee, J. C., Ragsdale, D. S., Scheuer, T., and Catterall, W. A. (1995) *J. Biol. Chem.* **270**, 12025–12034
- Cannon, S. C., and Strittmatter, S. M. (1993) *Neuron* **10**, 317–326
- McPhee, J. C., Ragsdale, D. S., Scheuer, T., and Catterall, W. A. (1998) *J. Biol. Chem.* **273**, 1121–1129
- Vedantham, V., and Cannon, S. C. (2000) *Biophys. J.* **78**, 2943–2958
- Wright, S. N., Wang, S. Y., and Wang, G. K. (1998) *Mol. Pharmacol.* **54**, 733–739
- French, R. J., Prusak-Sochaczewski, E., Zamponi, G. W., Becker, S., Kularatna, A. S., and Horn, R. (1996) *Neuron* **16**, 407–413
- French, R. J., and Dudley, S. C. J. (1999) *Methods Enzymol.* **294**, 575–605
- Fleiderovich, I. A., Friedman, A., and Gutnick, M. J. (1996) *J. Physiol. (Lond.)* **493**, 83–97
- Ruff, R. L., Simoncini, L., and Stühmer, W. (1987) *J. Physiol. (Lond.)* **383**, 339–348
- Pu, J., Balsler, J. R., and Boyden, P. A. (1998) *Circ. Res.* **83**, 431–440
- Pu, J., and Boyden, P. A. (1997) *Circ. Res.* **81**, 110–119
- Ren, D., Navarro, B., Xu, H., Yue, L., Shi, Q., and Clapham, D. E. (2001) *Science* **294**, 2372–2375
- Heinemann, S. H., Terlau, H., Stühmer, W., Imoto, K., and Numa, S. (1992) *Nature* **356**, 441–443